HHS Public Access

Author manuscript

Mol Cell Neurosci. Author manuscript; available in PMC 2018 July 01.

Published in final edited form as:

Mol Cell Neurosci. 2017 July ; 82: 23–34. doi:10.1016/j.mcn.2017.04.010.

Altered Temporal Lobe White Matter Lipid Ion Profiles in an Experimental Model of Sporadic Alzheimer;s Disease

Ming Tong[1,2,4], **Raiane Leão**[10], **Gina V. Vimbela**[9], **Emine B. Yalcin**[1], **Jared Kay**[1], **Alexander Krotow**[8], and **Suzanne M. de la Monte**[1,2,3,4,5,6,7]

[1]Liver Research Center, Rhode Island Hospital and the Warren Alpert Medical School of Brown University, Providence, RI

[2]Division of Gastroenterology, Rhode Island Hospital and the Warren Alpert Medical School of Brown University, Providence, RI

[3]Division of Neuropathology, Rhode Island Hospital and the Warren Alpert Medical School of Brown University, Providence, RI

[4]Department of Medicine, Rhode Island Hospital and the Warren Alpert Medical School of Brown University, Providence, RI

[5]Department of Pathology, Rhode Island Hospital and the Warren Alpert Medical School of Brown University, Providence, RI

[6]Department of Neurology, Rhode Island Hospital and the Warren Alpert Medical School of Brown University, Providence, RI

[7]Department of Neurosurgery, Rhode Island Hospital and the Warren Alpert Medical School of Brown University, Providence, RI

[8]Pathobiology Graduate Program, Brown University

[9]Department of Chemical Engineering, California State University, Long Beach, CA

[10]Federal University of Minas Gerais, Belo Horizonte, Minas Gerais, Brazil

Abstract

Background—White matter is an early and important yet under-evaluated target of Alzheimer's disease (AD). Metabolic impairments due to insulin and insulin-like growth factor resistance contribute to white matter degeneration because corresponding signal transduction pathways maintain oligodendrocyte function and survival.

Methods—This study utilized a model of sporadic AD in which adult Long Evans rats administered intracerebral streptozotocin (i.c. STZ) developed AD-type neurodegeneration.

Correspondence to Dr. Suzanne M. de la Monte, MD, MPH, Pierre Galletti Research Building, Rhode Island Hospital, 55 Claverick Street, Room 419, Providence, RI 02903. Tel: 401-444-7364; Fax: 401-444-2939; Suzanne_DeLaMonte_MD@Brown.edu.

Temporal lobe white matter lipid ion profiles were characterized by matrix-assisted laser desorption/ionization-imaging mass spectrometry (MALDI-IMS).

Results—Although the lipid ion species expressed in the i.c. STZ and control groups were virtually identical, i.c. STZ mainly altered the abundances of various lipid ions. Correspondingly, the i.c. STZ group was distinguished from control by principal component analysis and data bar plots. i.c. STZ mainly reduced expression of lipid ions with low m/z's (less than 810) as well as the upper range m/z lipids (m/z 964–986), and increased expression of lipid ions with m/z's between 888 and 937. Phospholipids were mainly included among the clusters inhibited by i.c. STZ, while both sulfatides and phospholipids were increased by i.c. STZ. However, Chi-Square analysis demonstrated significant i.c. STZ-induced trend reductions in phospholipids and increases in sulfatides ($P<0.00001$).

Conclusions—The i.c. STZ model of sporadic AD is associated with broad and sustained abnormalities in temporal lobe white matter lipids. The findings suggest that the i.c. STZ model could be used for pre-clinical studies to assess therapeutic measures for their ability to restore white matter integrity in AD.

Key terms

Alzheimer; white matter degeneration; Streptozotocin; MALDI; imaging mass spectrometry

Introduction

Alzheimer's disease (AD) is manifested by progressive behavioral changes, loss of recent memory, and declines in executive and cognitive functions (McKhann et al., 2011). The characteristic neuropathological changes in AD include brain accumulations of hyper-phosphorylated tau (pTau)-containing cytoskeletal lesion, and increased amyloid-beta (Aβ42) deposits in plaques, vessels, and neurons (Kalaria and Ballard, 1999; Viola and Klein, 2015). However, other more extensive and universal pathologies, including atrophy of white matter (WM), loss of neurons and synaptic terminals, neuro-inflammation, reactive astrocytosis, micro-vascular disease, and increased cellular stress with activation of the unfolded protein response (de la Monte, 2016; Hyman et al., 2012; Montine et al., 2012; Nelson et al., 2012) have received relatively little attention. Failure to attend to the full spectrum of disease could account for the persistent difficulties in rendering accurate diagnoses and repeated failure of clinical trials designed to treat just one aspect of AD (de la Monte, 2016).

WM atrophy and degeneration in AD was first characterized in 1986 by Brun and Englund (Brun and Englund, 1986a, b) and subsequently shown to represent an early abnormality that emerged in pre-clinical stages of disease (de la Monte, 1989). Its main histopathological features include pallor of myelin staining with Luxol fast blue dye due to decreased myelin density, attrition or rarefaction of axons, reduced population of oligodendrocytes, reactive gliosis (scarring), and vascular degeneration (Brickman et al., 2008; Brilliant et al., 1995; Brun and Englund, 1986a; Burns et al., 2005; de la Monte, 1989; Englund, 1998; Sjobeck and Englund, 2003; Sjobeck et al., 2005). In addition, WM atrophy in AD has been linked to increased accumulation of $A\beta_{1–40}$ and $A\beta_{1–42}$ (Roher et al., 2002).

WM is largely composed of lipid-rich myelin sheaths that are synthesized and maintained by oligodendrocytes. The wrapping of myelin sheaths around axons provides insulation, ensuring efficient electrochemical conductivity. Impaired function or death of oligodendrocytes disrupts myelin homeostasis, leading to myelin loss and compromised neurotransmission, plasticity and cognition. Mechanistically, myelin breakdown could be mediated by increased susceptibility of oligodendrocytes to free radical and other types of metabolic injury (Bartzokis, 2004).

Major CNS WM lipids include cholesterol, glycosphingolipids, i.e. cerebrosides (galactosylceramide, galactocerebroside), sulfatides (sulfated galactocerebroside, sulfogalactosylceramide), and gangliosides, and phospholipids, consisting of glycerophospholipids (phosphatidic acid (PA), phosphatidylcholine (PC), phosphatidylethanolamine (PE), phosphatidylglycerol (PG), phosphatidylinositol (PI), phosphatidylserine (PS) and plasmalogens) and sphingomyelin (Quarles et al., 2006). Sphingomyelin is composed of ceramide plus a phosphocholine or phosphoethanolamine polar head group (Quarles et al., 2006). Abnormal metabolism and expression of various lipids, including phospholipids and sulfatides occur in a broad range of CNS diseases (Takahashi and Suzuki, 2012). In AD, WM cholesterol, fatty acids, myelin basic protein, and myelin proteolipid protein levels are reduced (Roher et al., 2002; Wang et al., 2004) and sulfatides in both gray and WM are substantially diminished (Han et al., 2002).

Although the mechanisms and consequences of aberrant myelin lipid expression are not well understood, some effects can be predicted based on specific lipid functions. For example, the impairments in intracellular signaling associated with membrane phospholipid deficiencies correlate with their regulatory functions in lipid rafts and membrane receptors. Sulfatides, localized on the extracellular leaflet of myelin plasma membranes and synthesized through sulfonation of galactocerobroside (Vos et al., 1994), regulate neuronal plasticity, memory, myelin maintenance, protein trafficking, adhesion, glial-axonal signaling, insulin secretion, and oligodendrocyte survival (Takahashi and Suzuki, 2012; Vos et al., 1994). Correspondingly, reductions in membrane sulfatide disrupt myelin sheath structure and function, and compromise neuronal conductivity (Kolesnick and Kronke, 1998). Sulfatide degradation via increased galactosylceramidase, sulfatidase or aryl sulfatase activities yields ceramides (Eckhardt, 2008; Sundaram et al., 1995; Vos et al., 1994) that promote neuroinflammation, reactive oxygen species formation, apoptosis, and dysregulated signaling through cell survival and metabolic pathways (Kolesnick and Kronke, 1998).

Despite abundant information about AD’s adverse effects on WM, the biochemical nature of its degeneration has not been well characterized due to the lack of suitable tools for efficiently studying pathologic alterations in lipid-rich myelin. Fortunately, over the past several years, major advances in technology and computational science have facilitated extension of Matrix Assisted Laser Desorption Ionization Imaging Mass Spectrometry (MALDI-IMS) to human research. MALDI-IMS is used for in situ imaging of lipids, proteins, and adducts for correlation with histopathology and molecular pathology (in situ hybridization and immunohistochemistry) (Caprioli et al., 1997). Instruments equipped with an Nd:YAG Smartbeam laser enable time of flight (TOF; m/z) analysis for specific identification of molecules (Yalcin and de la Monte, 2015).

For this research, we utilized MALDI-IMS to characterize temporal lobe WM myelin lipid profile abnormalities in an intracerebral Streptozotocin (i.c. STZ) model of neurodegeneration. Although STZ is best known for its toxic effects on beta cells in pancreatic islets and production of Type 1 diabetes mellitus, at low doses it causes Type 2 diabetes with peripheral insulin resistance (Bolzan and Bianchi, 2002; Koulmanda et al., 2003; Wang et al., 2011; Yan et al., 2008), and when administered i.c., it causes AD-type neurodegeneration without damaging pancreatic islets or reducing pancreatic production of insulin (Blass et al., 2002; Blum-Degen et al., 1995; de la Monte et al., 2006; de la Monte et al., 2017; Gasparini et al., 2002; Lester-Coll et al., 2006). The rationale for employing the i.c. STZ model is that substantial evidence indicates that the major early abnormalities in AD include reductions in brain glucose metabolism, insulin/IGF trophic factor levels, and insulin/IGF-1 signaling through phosphoinositol-3-kinase (PI3K)-Akt pathways that regulate cell survival, energy metabolism, neuronal plasticity and WM integrity (de la Monte and Tong, 2014; de la Monte and Wands, 2008; Rivera et al., 2005; Steen et al., 2005; Talbot et al., 2012). Regarding WM, oligodendrocyte survival and function are regulated by insulin and insulin-like growth factor type 1 (IGF-1) signaling (Barres et al., 1993; Carson et al., 1993; Chesik et al., 2008) and brain diseases linked to insulin and IGF-1 trophic factor deficiencies or receptor resistances are associated with WM pathology (de la Monte, 2009, 2012, 2016; de la Monte et al., 2009). The i.c. STZ model is widely used because it produces neurobehavioral, histopathological, molecular, and biochemical abnormalities that mimic most aspects of sporadic AD, including amyloid-β deposition, pTau accumulations, cortical-limbic pathway degeneration, deficits in spatial learning and memory, neuro-inflammation, increased oxidative stress and WM degeneration (Akinola et al., 2015; de la Monte and Wands, 2008; Paidi et al., 2015; Salkovic-Petrisic et al., 2013; Tong et al., 2016a; Wang et al., 2014).

Methods

Experimental Model

A sporadic AD model was generated in 4-week old male Long Evans rats (8/group) by administration of i.c. STZ under ketamine/xylocine anesthesia (de la Monte et al., 2017; Lester-Coll et al., 2006; Tong et al., 2016a; Tong et al., 2016b). Control rats were given i.c. saline. The experiment was terminated on Day 28. Temporal lobes were dissected, snap frozen and stored at −80°C.

Matrix-assisted laser desorption/ionization imaging mass spectrometry (MALDI-IMS)

Frozen temporal lobes were equilibrated to −20°C in the cabinet of a Leica CM 3050 cryostat (Nossloch, Germany) and then mounted with optimum and consistent orientation onto cryostat chucks using a small drop of Tissue-Tek® optimal cutting temperature (OCT) compound (Sakura Finetek, Torrance, CA), such that none of the OCT contaminated the cut sections or slides. Cryostat sections (10 μm thick) were thaw mounted onto indium tin oxide (ITO) coated glass slides (Delta Technologies, Loveland, CO) and prepared for lipid analysis by sublimation coating with 200 ± 13 mg/cm^2 2,5-dehydroxybenzoic acid (DHB; Sigma-Aldrich Co, St. Louis, MO) as a thin uniform layer of matrix (Angel et al., 2012; Yalcin and de la Monte, 2015). The tissue sections were dehydrated for 1 hour in a vacuum desiccator,

then washed 5 times with 50 mM, pH 6.4 ammonium formate (150 μl/slide/wash-5 sec each) to remove salts and enhance sensitivity during spectra acquisition (Yalcin et al., 2015a; Yalcin et al., 2015b). The slides were again dried in a vacuum dessicator for 30 minutes.

Imaging experiments were performed using a reflectron geometry MALDI-time of flight (TOF)/TOF mass spectrometer (Ultraflextreme, Bruker Daltonics, Bremen, Germany). For analysis, a Smartbeam II Nd:YAG laser was focused onto ~100 μM^2 areas. Imaging data were acquired with the mass range set to 60–2000 Da by summing 500 shots/array position at a laser repetition rate of 1000 Hz and 25% power. To evaluate lipid profiles, imaged data were collected in the negative ion mode at a lateral resolution of 100 μM.

Data Analysis

Standardized regions of interest in adjacent histological sections stained with Luxol fast blue-Hematoxylin and Eosin (LHE) were co-registered with the MALDI-TOF image. MALDI data were processed using FlexAnalysis v3.4 (Bruker Daltonics, Billerica, MA) and visualized with FlexImaging software v4.0 (Bruker Daltonics, Billerica, MA). Results were normalized to total ion counts to prevent ion suppression and variation across tissue sections or matrix preparations (Jackson et al., 2007; Yalcin et al., 2015a; Yalcin et al., 2015b). Statistical analyses were performed using ClinProTools v3.0 (Bruker Daltonics, Billerica, MA). Phospholipids and sphingolipids were identified by comparing precursor and product ion m/z values with those catalogued in the LIPID MAPS database (http://www.lipidmaps.org/tools/index.html) and confirmed by tandem mass spectrometry (MS/MS) in the LIFT-TOF/TOF mode. In addition, lipid assignments were made based on published reports.

Inter-group comparisons were made using principal component analysis (PCA) and data bar plots with the goals of reducing dimensionality of the data sets while retaining the information present within the data corresponding to intensities and defined masses of expressed lipids. The PCA algorithm utilized reduced the number of dependent variables in each spectral set by replacing groups of intercorrelated variables with a single new variable (Shao et al., 2012). Data bar plots scaled by calculating mean percentage changes in lipid ion expression (m/z's 600–1200) were generated in R Version 3.2 using the ggplot2 module. Differences in the mean lipid ion expression levels were compared using Student T-tests with a 5% false discovery correction. In addition, Chi-square, fractional chi-square, and Cochran-Armitage tests were used to assess proportional alterations in lipid subtypes associated with i.c. STZ treatment.

Results

Characteristics of the Model

The characteristics of the model have already been reported (de la Monte et al., 2017; de la Monte et al., 2016; Tong et al., 2016a; Tong et al., 2016b). In brief, i.c. STZ caused sustained deficits in motor function (rotarod) (Tong et al., 2016b) and performance on spatial learning and memory tasks (Morris Water Maze) (Tong et al., 2016a). Neurodegeneration was associated with brain atrophy, neuronal loss, white matter degeneration, gliosis,

neuroinflammation, and increased levels of amyloid-beta, phospho-Tau, and ubiquitin immunoreactivity in the temporal lobe (de la Monte et al., 2017). In addition, the i.c. STZ treatments impaired signaling through the insulin and IGF-1 receptors, insulin receptor substrate proteins, and downstream pathways through phosphoinositol-3-kinase (PI3K)-Akt, and mTOR (de la Monte et al., 2017), and substantially altered expression of both immature and mature oligodendrocyte myelin associated genes and proteins (de la Monte et al., 2016).

Temporal Lobe WM Lipid Ion Profiles

Temporal lobe WM was subjected to MALDI-IMS in the negative ion mode. The Peak Statistic report identified 158 lipid ions with mass/charge (m/z) ratios between 648.92 and 1046.7 in all samples, and 8 others that were detected in either control (n=1) or i.c. STZ (n=7) brains (Table 1). Lipid assignments were made by comparing the precursor and product ion m/z values with those catalogued in the LIPID MAPS database and confirmed by MS/MS as previously described (Yalcin et al., 2015a; Yalcin et al., 2015b). Alternatively, the lipid ion assignments were made based on published reports (Dreisewerd et al., 2007; Eckhardt et al., 2007; Fernandez-Lima et al., 2011; Gode and Volmer, 2013; Hsu and Turk, 2000; Shanta et al., 2011).

Those analyses revealed that 1 PS was detected only in control brains, and 2 PS, 2 PE, 1 PI, 1 ST and 1 lipid that was not identified were differentially expressed in i.c. STZ WM (Table 1). All 8 lipid ions were expressed at low levels. The 158 lipid ions that were detected in both groups included 39 (24.7%) were sulfatides, among which 12 (30.8%) were C13-isotopes; 3 (1.9%) were ceramides, 1 (33%) of which was a C13-isotope of ceramide; 86 (54.4%) were phospholipids, among which 25 (29.1%) were C-13 isotopes of phospholipid ions; and 20 (12.7%) were not identified (Table 2). Note that the percentages of C13 stable isotopes were similar for the main lipid classes. In addition, it is likely that ceramides were under-represented since they are optimally detected in the positive rather than negative ion mode (Berry et al., 2011; Lohmann et al., 2010). Most of the 86 phospholipids were further characterized as PI (n=46; 53.4%), PS (n=26; 30.2%), PE (n=9; 10.4%), or PG (n=3; 3.5%); however, 2 (2.3%) phospholipids could not be further identified. Initial assessments of i.c. STZ's effect on WM lipid ion expression were made by comparing the peak intensity/area versus m/z profiles whereby higher peak intensity and area-under-curve values reflected greater abundances of specific lipids. Using this approach, the lipid ion profiles in control and i.c. STZ samples appeared quite similar, indicating that of the inter-group differences were most likely due to alterations in relative abundance rather than lipid composition (Figure 1).

Principal Component Analysis (PCA)

PCA was used to compare the groups with respect their overall patterns of lipid ion expression. The 3-D and 2-D plots demonstrated both overlapping and distinct distribution profiles for control and i.c. STZ samples (Figure 2). The overlapping components reflect shared expression of lipid ions, whereas the clearly separated regions depict long-term or sustained differential effects of i.c. STZ on WM lipid ions. Therefore, i.c. STZ altered expression of a subset of lipid ions.

Effects of i.c. STZ on Lipid Subtypes

To assess the effects of i.c. STZ on the expression levels of individual lipid ions, the mean percentage change in peak intensity (reflecting lipid ion abundance) was calculated for each of the 158 lipids detected (n=8 samples/experimental group). Data bar plots generated with the R Ggplot2 module illustrate relative effects of i.c. STZ on temporal lobe WM lipid ions (Figure 3). Bars extended to the left of the median vertical axis indicate i.c. STZ-induced reductions in the expression of specific lipid ions, whereas those to the right reflect i.c. STZ associated increases in lipid ion expression. The i.c. STZ-induced mean increases in lipid ion expression ranged from 0.05 to 12.6 percent, and reductions ranged from 0.05 to 12.1 percent. Inter-group differences were assessed by T-test analysis with 5% false discovery rate.

Results sorted by ascending m/z values demonstrate that most of i.c. STZ-induced reductions in lipid ion expression affected ions with m/z's below 809 and between 964 and 986 (Figure 3A; Table 3A). In contrast, i.c. STZ-induced increases in lipid ion abundance were distributed in 4 clusters ranging from: 1) 870.9 to 895.8; 2) 900.8 to 921.9; 3) 926.8 to 938.8; and 4) 958.8 to 963.8 (Figure 3A; Table 3A). Re-sorting of the data bar plot in ascending order of percentage change in lipid abundance revealed which lipid subtypes were most differentially altered in expression by i.c. STZ (Figure 3B; Table 3B). T-Test analysis detected significant differences ($P<0.05$) or statistical trends ($0.10>P>0.50$) for just 15 (9.5%) of the 158 lipid ions. All 5 of those reduced relative to control were phospholipids, including PIP(38:4) and its C13 isotope, PE(38:5) and its C13 isotope, and PG(34:1). In contrast, 9 of the 10 that were increased (significant or trend-wise) were sulfatides including C13 isotopes or hydroxylated forms. In addition, a statistical trend increase in lipid abundance was observed for the C13 isotope of PI(38:1) (Figure 3, Table 3). All significant and trend differences were greater than 5% increases relative to control. Failure to reach a statistical trend or statistical significance despite similar degrees of increased or reduced lipid expression was mainly due to larger within-group variances rather than directional responses. However, the data bar plots in Figures 3A and 3B clearly show clustered and similar patterned responses to i.c. STZ among lipid subtypes.

To determine how i.c. STZ altered the expression of different lipid ion subtypes, the proportional increases or reductions in temporal lobe WM phospholipids, sulfatides, C13-stable isotopes of sulfatides or phospholipids, and uncharacterized lipids were calculated (Table 4). Data were binned into 5 groups corresponding to i.c. STZ-induced changes in lipid ion abundance as follows: 1) greater 5% increases; 2) between 1% and 5% increases; 3) no change, i.e. less than 1% increases or decreases; 4) between 1% and 5% decreases; and 5) greater than 5% reductions and analyzed using the Pearson's Chi-square test (2-sided) and Cochran-Armitage Trend Test. Among the 158 lipid ions detected by MALDI-IMS, i.c. STZ increased expression of 32 (20.3%) by more than 5%, and 37 (23.4%) from 1% and 5%, but decreased expression of 11 (7%) by more than 5%, and 40 (25.3%) from 1% to 5%. Only 38 (24.1%) ions were similarly expressed (less than 1% difference) in i.c. STZ and control samples (Table 4).

Chi-square tests demonstrated that i.c. STZ significantly altered the percentages of phospholipids, sulfatides, and unidentified lipids that were either increased or decreased in

abundance relative to control (χ^2= 19.46; P=0.0126) (Figure 4A). Analysis of just the ST and phospholipid responses (omitting unidentified lipids) revealed highly significant effects of i.c. STZ (χ^2=20.46; P=0.0004) with disproportionately greater inhibition of phospholipids compared with STs (P=0.00001). Comparison of i.c. STZ's effects on subdivided ST and phospholipid C12 and C13 isotope lipids demonstrated trend effects on C12 (χ^2=9.29, P=0.054) and significant effects on C13 isotopes (χ^2=17.33, P=0.0017). However, the Cochran-Armitage Test revealed a significant increasing trend for C12 phospholipids such that disproportionately higher percentages were inhibited relative to ST (P=0.006), and conversely, disproportionately greater percentages of C13 phospholipids with increased expression compared with ST (P=0.00003).

Fractional Chi-square tests showed that i.c. STZ disproportionately increased the percentages of STs in which expression was elevated between 1% and 5% above control (χ^2 =11.6; P=0.003), and percentages of phospholipids that had greater than 5% reductions in their abundance relative to control (χ^2=8.36; P=0.015) (Figure 4C). Further evidence that i.c. STZ disproportionately inhibited expression of phospholipids compared with ST was provided by the significantly greater percentages of phospholipids (C12 and C13 isotopes combined) with 1% to 5% (χ^2=8.27, P=0.04) or greater than 5% (χ^2=23.07, P<0.0001) reductions in abundance relative to control (Table 4). Pearson's Chi-Square analysis of i.c. STZ's effects on overall phospholipid expression reached a statistical trend (P=0.054). However, after removing the PG data which contributed just 3 lipids, the results were statistically significant (χ^2=17.43, P=0.026) (Figure 4B). Fractional Chi-square tests demonstrated significant i.c. STZ's effects on the proportions of PE, PI and PS that were increased by more than 5% or between 1% and 5%, or decreased by more than 5% relative to control (Figure 4C). The corresponding responses included increased expression in 36% of PI and 27% of PS versus none of the PE lipids, and greater than 5% reductions in 15% of PI and 22% of PE, but none of the PS lipids (Figure 4B).

Discussion

AD like diabetes mellitus is associated with insulin resistance, except brain rather than skeletal muscle is the principal target organ. In the brain, insulin is a key regulator of glucose utilization and signal transduction networks that mediate cell growth, plasticity, metabolism, neuronal survival, myelin maintenance and acetylcholine biosynthesis, and it inhibits oxidative stress and apoptosis (Craft, 2006, 2007; de la Monte, 2009, 2012; de la Monte and Wands, 2005, 2008). Proof of principle for this concept has been provided by experiments in which i.c. administration of STZ, a pro-diabetes toxin, was shown to impair spatial learning and memory and cause brain atrophy with histopathological, molecular, and biochemical abnormalities associated with AD neurodegeneration in humans (Lester-Coll et al., 2006). Similarly, with the model used for studies of temporal lobe WM lipids, deficits in spatial learning and memory, AD-type neuropathology including amyloid-beta, phospho-tau, and ubiquitin accumulations in brain, and WM degeneration with impaired expresion of myelin-associated genes and proteins have been reported (de la Monte et al., 2017; de la Monte et al., 2016; Tong et al., 2016a; Tong et al., 2016b).

WM degeneration, characterized by atrophy, loss of myelin and myelinated fibers, and gliosis (Brun and Englund, 1986a; de la Monte, 1989; Sjobeck and Englund, 2003; Sjobeck et al., 2005; Wang et al., 2004), develops early in the course of AD. Loss of myelin and myelinated fibers adversely affects neuronal conductivity, plasticity, and brain function. Although the mechanisms are not well understood, WM pathology in AD could be mediated by impairments in insulin and IGF signaling since these pathways support oligodendrocyte survival and function, including myelin maintenance (Barres et al., 1993; Carson et al., 1993; Chesik et al., 2008). Since myelin is largely composed of lipids, metabolic dysregulation or degeneration of oligodendrocytes could lead to altered WM lipid composition which could contribute to cognitive decline. The present study utilized an i.c. STZ model to interrogate the extent to which WM myelin lipid profiles were modulated by brain metabolic dysfunction linked to impairments in insulin and IGF signaling. Apart from its many parallels with human AD, the rationale for using the i.c. STZ model over the standard genetically manipulated models is that the latter are not known to produce the full spectrum of molecular and pathological abnormalities (including WM degeneration) that occur in sporadic AD, which accounts for the vast majority of cases.

MALDI-IMS was used to acquire lipidomics data and examine effects of i.c. STZ on temporal lobe WM lipid profiles. One limitation of MALDI is that molecules are not separated prior to detection, making structural assignment of isobaric compounds quite challenging. On the other hand, the approach is more feasible for studying diseases since it enables mapping of biochemical with histopathological abnormalities. Moreover, since neurodegeneration is associated with oxidative injury, extraction procedures may lead to further artefactual molecular damage and generate differences that were not present in situ. For lipid identification, we performed tandem mass spectrometry (MS/MS) following IMS. The product ion spectra matched with individual lipids catalogued in LIPIDMAPS. However, due to their low abundances, MS/MS analysis of many lipids was inconclusive, leading us to make assignments based on published data in which the analyses of rodent brains were performed using higher resolution mass spectrometry, such as Fourier transform ion cyclotron resonance or tandem mass spectrometry. For the few instances in the Lipid MAPS search yielded isobaric lipid species, e.g. PC(16:0/24:1(15Z)) and PC(18:0/22:1(13Z)), instead of specifying the number of carbon atoms in each fatty acyl chain or positions of double bonds, we identified the lipid as PC(40:1).

The two main overall findings were that 8 low-abundance, predominantly phospholipid ions exhibited non-overlapping expression between the i.c. STZ and control groups, and the i.c. STZ treatments resulted in clustered (patterned) alterations in the expression levels of sulfatides and different phospholipids. Although the significance of differentially expressed lipids in relation to disease states is not yet understood, such findings highlight the potential contributions of dysregulated lipid metabolism as mediators or biomarkers of pathology. The altered patterns of lipid expression caused by i.c. STZ mainly corresponded to clustered shifts (increases or reductions) in relative abundance. Individually specific inter-group differences were detected for only 15 (9.5%) lipids. However, taken together, the findings are internally consistent in that both show i.c. STZ inhibition of mainly phospholipids and stimulation of sulfatides, including their corresponding C13 isotopes. These findings correspond with the previous findings of modest shifts in brain levels of individual

phospholipids and sphingolipids in humans with AD (Chan et al., 2012), and the considerable alterations in AD brain WM sphingolipid and phospholipid compositions (Brun and Englund, 1986a; de la Monte et al., 2012; de la Monte and Tong, 2014; Gottfries et al., 1996; Han et al., 2002; He et al., 2010; Wood, 2012).

Membrane phospholipids are integral components of plasma membranes, regulating receptor functions and microdomains (lipid rafts). Reduced phospholipid levels have been correlated with insulin resistance states (Ikonen and Vainio, 2005; Vainio et al., 2005). Therefore, the finding of disproportionately reduced phospholipid ion expression in WM of i.c. STZ treated rats could represent a consequence of brain insulin resistance. Furthermore, the reductions in WM phospholipids, including PI and PE, may have exacerbated disruption of downstream metabolic signaling, as occurs in AD (Craft, 2006, 2007; Rivera et al., 2005; Talbot et al., 2012).

The i.c. STZ mediated increases in temporal lobe WM ST expression are of interest because they are largely discordant with the findings in human AD brains which exhibit sulfatide depletion rather than accumulation (Brun and Englund, 1986a; de la Monte et al., 2012; de la Monte and Tong, 2014; Gottfries et al., 1996; Han et al., 2002; He et al., 2010; Wood, 2012). Sulfatides are glycosphingolipids synthesized by oligodendrocytes via sulfonation of galactocerobroside, which is generated from ceramide and galactose. Galactosylceramidase and sulfatidase can enzymatically degrade sufatides to ceramide and sulfate (Eckhardt, 2008; Vos et al., 1994). Sulfatide expression marks oligodendrocyte function as these lipids are needed for normal protein trafficking, neuronal plasticity, memory, adhesion, myelin maintenance, glial-axonal signaling, insulin secretion, and oligodendrocyte survival (Takahashi and Suzuki, 2012). Reductions in membrane sulfatide content can cause structural and functional disruption of myelin sheaths and impair neuronal conductivity. Increased degradation of sulfatide back to ceramide can lead to neuro-inflammation, generation of reactive oxygen species, and apoptosis (Kolesnick and Kronke, 1998). Correspondingly, increased brain ceramide levels have been linked to cognitive impairment and neurodegeneration due to increased oxidative stress, neuro-inflammation, insulin resistance, and deficits in oligodendrocyte myelin-associated gene expression (de la Monte et al., 2010; Tong and de la Monte, 2009). These pathogenic processes have been established as features of AD (de la Monte et al., 2012), and could be mediated by sulfatide deficiency (Han et al., 2002) and/or ceramide accumulation (de la Monte et al., 2012). Of further note is that abnormal metabolism and expression of sulfatides occur in other disease states including Parkinson’s disease, metachromatic leukodystrophy, diabetes mellitus, epilepsy, and viral infection (Takahashi and Suzuki, 2012). Mechanistically, sulfatide depletion in AD could be due to reductions in cerebrosides, the precursors of sulfatides, rather than altered expression of enzyme or enzymatic dysfunction (Wood, 2012).

One potential explanation for the discordant overall i.c. STZ-associated increases in sulfatide vis-à-vis their broad reductions in AD is that the severity of neurodegeneration in the model was far less than observed in postmortem human brains, perhaps due to the relatively short duration of the model. If this is the case, the findings herein would argue that reductions in WM phospholipid expression precede sulfatide depletion, and that enhanced expression of sulfatides could represent an early compensatory response to brain metabolic dysfunction. In

support of this concept is the finding that while several of the 39 sulfatides were modestly decreased in expression, 2 (m/z 792.84 and 806.82) were substantially down-regulated in the i.c. STZ brains. Questions regarding the time course x nature of altered WM myelin lipid expression in relation to neurodegeneration could be addressed by studying human brains with different degrees (durations) of AD and i.c. STZ-treated brains after more prolonged periods of observation.

An additional potential explanation for the discordant experimental and human data is that molecular and biochemical responses to disease states and their corresponding effects may differ among the species. For example, in other experimental models increased sulfatide accumulation was linked to progressive myelin loss and neurological deficits (Ramakrishnan et al., 2007). In addition, elevated sulfatides in brain have been associated with increased neuro-inflammation (Jeon et al., 2008), and neuroinflammation is a feature of both AD (Agostinho et al., 2010; Mehlhorn et al., 2000; Mrak, 2009) and the i.c. STZ model (de la Monte et al., 2017). In essence, the i.c. STZ model is associated with substantial alterations in both phospholipids and sulfatides, and while the abnormalities overlap with those observed in AD, distinct differences exist that could be attributed to the manner of disease induction, differential species responses, or disease time course/duration effects.

Acknowledgments

Supported by AA-011431 and AG-049510 from the National Institutes of Health

References

Agostinho P, Cunha RA, Oliveira C. Neuroinflammation, oxidative stress and the pathogenesis of Alzheimer's disease. Curr Pharm Des. 2010; 16:2766–2778. [PubMed: 20698820]

Akinola OB, Biliaminu SA, Adediran RA, Adeniye KA, Abdulquadir FC. Characterization of prefrontal cortex microstructure and antioxidant status in a rat model of neurodegeneration induced by aluminium chloride and multiple low-dose streptozotocin. Metab Brain Dis. 2015; 30:1531–1536. [PubMed: 26307418]

Angel PM, Spraggins JM, Baldwin HS, Caprioli R. Enhanced sensitivity for high spatial resolution lipid analysis by negative ion mode matrix assisted laser desorption ionization imaging mass spectrometry. Analytical chemistry. 2012; 84:1557–1564. [PubMed: 22243218]

Barres BA, Schmid R, Sendnter M, Raff MC. Multiple extracellular signals are required for long-term oligodendrocyte survival. Development (Cambridge, England). 1993; 118:283–295.

Bartzokis G. Age-related myelin breakdown: a developmental model of cognitive decline and Alzheimer's disease. Neurobiol Aging. 2004; 25:5–18. author reply 49–62. [PubMed: 14675724]

Berry KA, Hankin JA, Barkley RM, Spraggins JM, Caprioli RM, Murphy RC. MALDI imaging of lipid biochemistry in tissues by mass spectrometry. Chem Rev. 2011; 111:6491–6512. [PubMed: 21942646]

Blass JP, Gibson GE, Hoyer S. The role of the metabolic lesion in Alzheimer's disease. J Alzheimers Dis. 2002; 4:225–232. [PubMed: 12226541]

Blum-Degen D, Frolich L, Hoyer S, Riederer P. Altered regulation of brain glucose metabolism as a cause of neurodegenerative disorders? J Neural Transm Suppl. 1995; 46:139–147. [PubMed: 8821049]

Bolzan AD, Bianchi MS. Genotoxicity of streptozotocin. Mutat Res. 2002; 512:121–134. [PubMed: 12464347]

Brickman AM, Honig LS, Scarmeas N, Tatarina O, Sanders L, Albert MS, Brandt J, Blacker D, Stern Y. Measuring cerebral atrophy and white matter hyperintensity burden to predict the rate of cognitive decline in Alzheimer disease. Arch Neurol. 2008; 65:1202–1208. [PubMed: 18779424]

Brilliant M, Hughes L, Anderson D, Ghobrial M, Elble R. Rarefied white matter in patients with Alzheimer disease. Alzheimer Dis Assoc Disord. 1995; 9:39–46. [PubMed: 7605620]

Brun A, Englund E. Brain changes in dementia of Alzheimer's type relevant to new imaging diagnostic methods. Prog Neuropsychopharmacol Biol Psychiatry. 1986a; 10:297–308. [PubMed: 3492011]

Brun A, Englund E. A white matter disorder in dementia of the Alzheimer type: a pathoanatomical study. Ann Neurol. 1986b; 19:253–262. [PubMed: 3963770]

Burns JM, Church JA, Johnson DK, Xiong C, Marcus D, Fotenos AF, Snyder AZ, Morris JC, Buckner RL. White matter lesions are prevalent but differentially related with cognition in aging and early Alzheimer disease. Arch Neurol. 2005; 62:1870–1876. [PubMed: 16344345]

Caprioli RM, Farmer TB, Gile J. Molecular imaging of biological samples: localization of peptides and proteins using MALDI-TOF MS. Analytical chemistry. 1997; 69:4751–4760. [PubMed: 9406525]

Carson MJ, Behringer RR, Brinster RL, McMorris FA. Insulin-like growth factor I increases brain growth and central nervous system myelination in transgenic mice. Neuron. 1993; 10:729–740. [PubMed: 8386530]

Chan RB, Oliveira TG, Cortes EP, Honig LS, Duff KE, Small SA, Wenk MR, Shui G, Di Paolo G. Comparative lipidomic analysis of mouse and human brain with Alzheimer disease. J Biol Chem. 2012; 287:2678–2688. [PubMed: 22134919]

Chesik D, De Keyser J, Wilczak N. Insulin-like growth factor system regulates oligodendroglial cell behavior: therapeutic potential in CNS. J Mol Neurosci. 2008; 35:81–90. [PubMed: 18299999]

Craft S. Insulin resistance syndrome and Alzheimer disease: pathophysiologic mechanisms and therapeutic implications. Alzheimer Dis Assoc Disord. 2006; 20:298–301. [PubMed: 17132977]

Craft S. Insulin resistance and Alzheimer's disease pathogenesis: potential mechanisms and implications for treatment. Curr Alzheimer Res. 2007; 4:147–152. [PubMed: 17430239]

de la Monte SM. Quantitation of cerebral atrophy in preclinical and end-stage Alzheimer's disease. Ann Neurol. 1989; 25:450–459. [PubMed: 2774485]

de la Monte SM. Insulin resistance and Alzheimer's disease. BMB Rep. 2009; 42:475–481. [PubMed: 19712582]

de la Monte SM. Brain insulin resistance and deficiency as therapeutic targets in Alzheimer's disease. Curr Alzheimer Res. 2012; 9:35–66. [PubMed: 22329651]

de la Monte SM. Insulin Resistance and Neurodegeneration: Progress Towards the Development of New Therapeutics for Alzheimer's Disease. Drugs. 2016

de la Monte SM, Longato L, Tong M, Wands JR. Insulin resistance and neurodegeneration: roles of obesity, type 2 diabetes mellitus and non-alcoholic steatohepatitis. Curr Opin Investig Drugs. 2009; 10:1049–1060.

de la Monte SM, Re E, Longato L, Tong M. Dysfunctional pro-ceramide, ER stress, and insulin/IGF signaling networks with progression of Alzheimer's disease. J Alzheimers Dis. 2012; 30(Suppl 2):S217–229. [PubMed: 22297646]

de la Monte SM, Tong M. Brain metabolic dysfunction at the core of Alzheimer's disease. Biochem Pharmacol. 2014; 88:548–559. [PubMed: 24380887]

de la Monte SM, Tong M, Lester-Coll N, Plater M Jr, Wands JR. Therapeutic rescue of neurodegeneration in experimental type 3 diabetes: relevance to Alzheimer's disease. J Alzheimers Dis. 2006; 10:89–109. [PubMed: 16988486]

de la Monte SM, Tong M, Nguyen V, Setshedi M, Longato L, Wands JR. Ceramide-mediated insulin resistance and impairment of cognitive-motor functions. J Alzheimers Dis. 2010; 21:967–984. [PubMed: 20693650]

de la Monte SM, Tong M, Schiano I, Didsbury J. Improved Brain Insulin/IGF Signaling and Reduced Neuroinflammation with T3D-959 in an Experimental Model of Sporadic Alzheimer's Disease. J Alzheimers Dis. 2017; 55:849–864. [PubMed: 27802237]

de la Monte SM, Tong M, Vimbela G. Oligodendroglial and neuroglial molecular abnormalities in the intracerebral streptozotocin model of sporadic Alzheimer's Disease. J Alzheimer's Parkinsonism Dementia. 2016; 1:1–15.

de la Monte SM, Wands JR. Review of insulin and insulin-like growth factor expression, signaling, and malfunction in the central nervous system: relevance to Alzheimer's disease. J Alzheimers Dis. 2005; 7:45–61. [PubMed: 15750214]

de la Monte SM, Wands JR. Alzheimer's disease is type 3 diabetes-evidence reviewed. J Diabetes Sci Technol. 2008; 2:1101–1113. [PubMed: 19885299]

Dreisewerd K, Lemaire R, Pohlentz G, Salzet M, Wisztorski M, Berkenkamp S, Fournier I. Molecular profiling of native and matrix-coated tissue slices from rat brain by infrared and ultraviolet laser desorption/ionization orthogonal time-of-flight mass spectrometry. Analytical chemistry. 2007; 79:2463–2471. [PubMed: 17305311]

Eckhardt M. The role and metabolism of sulfatide in the nervous system. Molecular neurobiology. 2008; 37:93–103. [PubMed: 18465098]

Eckhardt M, Hedayati KK, Pitsch J, Lullmann-Rauch R, Beck H, Fewou SN, Gieselmann V. Sulfatide storage in neurons causes hyperexcitability and axonal degeneration in a mouse model of metachromatic leukodystrophy. J Neurosci. 2007; 27:9009–9021. [PubMed: 17715338]

Englund E. Neuropathology of white matter changes in Alzheimer's disease and vascular dementia. Dement Geriatr Cogn Disord. 1998; 9(Suppl 1):6–12.

Fernandez-Lima FA, Post J, DeBord JD, Eller MJ, Verkhoturov SV, Della-Negra S, Woods AS, Schweikert EA. Analysis of native biological surfaces using a 100 kV massive gold cluster source. Analytical chemistry. 2011; 83:8448–8453. [PubMed: 21967684]

Gasparini L, Netzer WJ, Greengard P, Xu H. Does insulin dysfunction play a role in Alzheimer's disease? Trends Pharmacol Sci. 2002; 23:288–293. [PubMed: 12084635]

Gode D, Volmer DA. Lipid imaging by mass spectrometry - a review. Analyst. 2013; 138:1289–1315. [PubMed: 23314100]

Gottfries CG, Karlsson I, Svennerholm L. Membrane components separate early-onset Alzheimer's disease from senile dementia of the Alzheimer type. International psychogeriatrics / IPA. 1996; 8:365–372.

Han X, DMH, McKeel DW Jr, Kelley J, Morris JC. Substantial sulfatide deficiency and ceramide elevation in very early Alzheimer's disease: potential role in disease pathogenesis. J Neurochem. 2002; 82:809–818. [PubMed: 12358786]

He X, Huang Y, Li B, Gong CX, Schuchman EH. Deregulation of sphingolipid metabolism in Alzheimer's disease. Neurobiology of aging. 2010; 31:398–408. [PubMed: 18547682]

Hsu FF, Turk J. Characterization of phosphatidylinositol, phosphatidylinositol-4-phosphate, and phosphatidylinositol-4,5-bisphosphate by electrospray ionization tandem mass spectrometry: a mechanistic study. Journal of the American Society for Mass Spectrometry. 2000; 11:986–999. [PubMed: 11073262]

Hyman BT, Phelps CH, Beach TG, Bigio EH, Cairns NJ, Carrillo MC, Dickson DW, Duyckaerts C, Frosch MP, Masliah E, Mirra SS, Nelson PT, Schneider JA, Thal DR, Thies B, Trojanowski JQ, Vinters HV, Montine TJ. National Institute on Aging-Alzheimer's Association guidelines for the neuropathologic assessment of Alzheimer's disease. Alzheimers Dement. 2012; 8:1–13. [PubMed: 22265587]

Ikonen E, Vainio S. Lipid microdomains and insulin resistance: is there a connection? Sci STKE. 2005; 2005:pe3. [PubMed: 15671480]

Jackson SN, Wang HY, Woods AS. In situ structural characterization of glycerophospholipids and sulfatides in brain tissue using MALDI-MS/MS. Journal of the American Society for Mass Spectrometry. 2007; 18:17–26. [PubMed: 17005416]

Jeon SB, Yoon HJ, Park SH, Kim IH, Park EJ. Sulfatide, a major lipid component of myelin sheath, activates inflammatory responses as an endogenous stimulator in brain-resident immune cells. J Immunol. 2008; 181:8077–8087. [PubMed: 19018000]

Kalaria RN, Ballard C. Overlap between pathology of Alzheimer disease and vascular dementia. Alzheimer Dis Assoc Disord. 1999; 13(Suppl 3):S115–123. [PubMed: 10609690]

Kolesnick RN, Kronke M. Regulation of ceramide production and apoptosis. Annual review of physiology. 1998; 60:643–665.

Koulmanda M, Qipo A, Chebrolu S, O'Neil J, Auchincloss H, Smith RN. The effect of low versus high dose of streptozotocin in cynomolgus monkeys (Macaca fascilularis). Am J Transplant. 2003; 3:267–272. [PubMed: 12614280]

Lester-Coll N, Rivera EJ, Soscia SJ, Doiron K, Wands JR, de la Monte SM. Intracerebral streptozotocin model of type 3 diabetes: relevance to sporadic Alzheimer's disease. J Alzheimers Dis. 2006; 9:13–33. [PubMed: 16627931]

Lohmann C, Schachmann E, Dandekar T, Villmann C, Becker CM. Developmental profiling by mass spectrometry of phosphocholine containing phospholipids in the rat nervous system reveals temporo-spatial gradients. J Neurochem. 2010; 114:1119–1134. [PubMed: 20524967]

McKhann GM, Knopman DS, Chertkow H, Hyman BT, Jack CR Jr, Kawas CH, Klunk WE, Koroshetz WJ, Manly JJ, Mayeux R, Mohs RC, Morris JC, Rossor MN, Scheltens P, Carrillo MC, Thies B, Weintraub S, Phelps CH. The diagnosis of dementia due to Alzheimer's disease: recommendations from the National Institute on Aging-Alzheimer's Association workgroups on diagnostic guidelines for Alzheimer's disease. Alzheimers Dement. 2011; 7:263–269. [PubMed: 21514250]

Mehlhorn G, Hollborn M, Schliebs R. Induction of cytokines in glial cells surrounding cortical beta-amyloid plaques in transgenic Tg2576 mice with Alzheimer pathology. Int J Dev Neurosci. 2000; 18:423–431. [PubMed: 10817926]

Montine TJ, Phelps CH, Beach TG, Bigio EH, Cairns NJ, Dickson DW, Duyckaerts C, Frosch MP, Masliah E, Mirra SS, Nelson PT, Schneider JA, Thal DR, Trojanowski JQ, Vinters HV, Hyman BT. National Institute on A, Alzheimer's A. National Institute on Aging-Alzheimer's Association guidelines for the neuropathologic assessment of Alzheimer's disease: a practical approach. Acta Neuropathol. 2012; 123:1–11. [PubMed: 22101365]

Mrak RE. Neuropathology and the neuroinflammation idea. J Alzheimers Dis. 2009; 18:473–481. [PubMed: 19584454]

Nelson PT, Alafuzoff I, Bigio EH, Bouras C, Braak H, Cairns NJ, Castellani RJ, Crain BJ, Davies P, Del Tredici K, Duyckaerts C, Frosch MP, Haroutunian V, Hof PR, Hulette CM, Hyman BT, Iwatsubo T, Jellinger KA, Jicha GA, Kovari E, Kukull WA, Leverenz JB, Love S, Mackenzie IR, Mann DM, Masliah E, McKee AC, Montine TJ, Morris JC, Schneider JA, Sonnen JA, Thal DR, Trojanowski JQ, Troncoso JC, Wisniewski T, Woltjer RL, Beach TG. Correlation of Alzheimer disease neuropathologic changes with cognitive status: a review of the literature. J Neuropathol Exp Neurol. 2012; 71:362–381. [PubMed: 22487856]

Paidi RK, Nthenge-Ngumbau DN, Singh R, Kankanala T, Mehta H, Mohanakumar KP. Mitochondrial Deficits Accompany Cognitive Decline Following Single Bilateral Intracerebroventricular Streptozotocin. Curr Alzheimer Res. 2015; 12:785–795. [PubMed: 26159195]

Quarles, RH., Macklin, WB., Morell, P. Myelin Formation, Structure and Biochemistry. 6. Elsevier; Philadelphia: 2006.

Ramakrishnan H, Hedayati KK, Lullmann-Rauch R, Wessig C, Fewou SN, Maier H, Goebel HH, Gieselmann V, Eckhardt M. Increasing sulfatide synthesis in myelin-forming cells of arylsulfatase A-deficient mice causes demyelination and neurological symptoms reminiscent of human metachromatic leukodystrophy. J Neurosci. 2007; 27:9482–9490. [PubMed: 17728461]

Rivera EJ, Goldin A, Fulmer N, Tavares R, Wands JR, de la Monte SM. Insulin and insulin-like growth factor expression and function deteriorate with progression of Alzheimer's disease: link to brain reductions in acetylcholine. J Alzheimers Dis. 2005; 8:247–268. [PubMed: 16340083]

Roher AE, Weiss N, Kokjohn TA, Kuo YM, Kalback W, Anthony J, Watson D, Luehrs DC, Sue L, Walker D, Emmerling M, Goux W, Beach T. Increased A beta peptides and reduced cholesterol and myelin proteins characterize white matter degeneration in Alzheimer's disease. Biochemistry. 2002; 41:11080–11090. [PubMed: 12220172]

Salkovic-Petrisic M, Knezovic A, Hoyer S, Riederer P. What have we learned from the streptozotocin-induced animal model of sporadic Alzheimer's disease, about the therapeutic strategies in Alzheimer's research. J Neural Transm (Vienna). 2013; 120:233–252. [PubMed: 22886150]

Shanta SR, Zhou LH, Park YS, Kim YH, Kim Y, Kim KP. Binary matrix for MALDI imaging mass spectrometry of phospholipids in both ion modes. Analytical chemistry. 2011; 83:1252–1259. [PubMed: 21244088]

Shao C, Tian Y, Dong Z, Gao J, Gao Y, Jia X, Guo G, Wen X, Jiang C, Zhang X. The Use of Principal Component Analysis in MALDI-TOF MS: a Powerful Tool for Establishing a Mini-optimized Proteomic Profile. Am J Biomed Sci. 2012; 4:85–101. [PubMed: 22229059]

Sjobeck M, Englund E. Glial levels determine severity of white matter disease in Alzheimer's disease: a neuropathological study of glial changes. Neuropathol Appl Neurobiol. 2003; 29:159–169. [PubMed: 12662323]

Sjobeck M, Haglund M, Englund E. Decreasing myelin density reflected increasing white matter pathology in Alzheimer's disease--a neuropathological study. Int J Geriatr Psychiatry. 2005; 20:919–926. [PubMed: 16163742]

Steen E, Terry BM, Rivera EJ, Cannon JL, Neely TR, Tavares R, Xu XJ, Wands JR, de la Monte SM. Impaired insulin and insulin-like growth factor expression and signaling mechanisms in Alzheimer's disease--is this type 3 diabetes? J Alzheimers Dis. 2005; 7:63–80. [PubMed: 15750215]

Sundaram SK, Fan JH, Lev M. A neutral galactocerebroside sulfate sulfatidase from mouse brain. J Biol Chem. 1995; 270:10187–10192. [PubMed: 7730322]

Takahashi T, Suzuki T. Role of sulfatide in normal and pathological cells and tissues. J Lipid Res. 2012; 53:1437–1450. [PubMed: 22619219]

Talbot K, Wang HY, Kazi H, Han LY, Bakshi KP, Stucky A, Fuino RL, Kawaguchi KR, Samoyedny AJ, Wilson RS, Arvanitakis Z, Schneider JA, Wolf BA, Bennett DA, Trojanowski JQ, Arnold SE. Demonstrated brain insulin resistance in Alzheimer's disease patients is associated with IGF-1 resistance, IRS-1 dysregulation, and cognitive decline. J Clin Invest. 2012; 122:1316–1338. [PubMed: 22476197]

Tong M, de la Monte SM. Mechanisms of ceramide-mediated neurodegeneration. J Alzheimers Dis. 2009; 16:705–714. [PubMed: 19387107]

Tong M, Deochand C, Didsbury J, de la Monte SM. T3D-959: A Multi-Faceted Disease Remedial Drug Candidate for the Treatment of Alzheimer's Disease. J Alzheimers Dis. 2016a; 51:123–138. [PubMed: 26836193]

Tong M, Dominguez C, Didsbury J, de la Monte SM. Targeting Alzheimer's Disease Neuro-Metabolic Dysfunction with a Small Molecule Nuclear Receptor Agonist (T3D-959) Reverses Disease Pathologies. J Alzheimers Dis Parkinsonism. 2016b; 6:238–244. [PubMed: 27525190]

Vainio S, Bykov I, Hermansson M, Jokitalo E, Somerharju P, Ikonen E. Defective insulin receptor activation and altered lipid rafts in Niemann-Pick type C disease hepatocytes. Biochem J. 2005; 391:465–472. [PubMed: 15943586]

Viola KL, Klein WL. Amyloid beta oligomers in Alzheimer's disease pathogenesis, treatment, and diagnosis. Acta Neuropathol. 2015; 129:183–206. [PubMed: 25604547]

Vos JP, Lopes-Cardozo M, Gadella BM. Metabolic and functional aspects of sulfogalactolipids. Biochim Biophys Acta. 1994; 1211:125–149. [PubMed: 8117740]

Wang DS, Bennett DA, Mufson EJ, Mattila P, Cochran E, Dickson DW. Contribution of changes in ubiquitin and myelin basic protein to age-related cognitive decline. Neurosci Res. 2004; 48:93–100. [PubMed: 14687885]

Wang JQ, Yin J, Song YF, Zhang L, Ren YX, Wang DG, Gao LP, Jing YH. Brain aging and AD-like pathology in streptozotocin-induced diabetic rats. J Diabetes Res. 2014; 2014:796840. [PubMed: 25197672]

Wang S, Kamat A, Pergola P, Swamy A, Tio F, Cusi K. Metabolic factors in the development of hepatic steatosis and altered mitochondrial gene expression in vivo. Metabolism. 2011; 60:1090–1099. [PubMed: 21310443]

Wood PL. Lipidomics of Alzheimer's disease: current status. Alzheimers Res Ther. 2012; 4:5. [PubMed: 22293144]

Yalcin EB, de la Monte SM. Review of matrix-assisted laser desorption ionization-imaging mass spectrometry for lipid biochemical histopathology. J Histochem Cytochem. 2015; 63:762–771. [PubMed: 26209083]

Yalcin EB, Nunez K, Cornett DS, de la Monte SM. Differential Lipid Profiles in Experimental Steatohepatitis: Role for Imaging Mass Spectrometry as a Diagnostic Aid. Journal of Drug and Alcohol Research. 2015a; 4:1–11.

Yalcin EB, Nunez K, Tong M, de la Monte SM. Differential Sphingolipid and Phospholipid Profiles in Alcohol and Nicotine-Derived Nitrosamine Ketone-Associated White Matter Degeneration. Alcohol Clin Exp Res. 2015b; 39:2324–2333. [PubMed: 26756797]

Yan AG, Ge ZY, Liu JX, Dong XX, Li HK, Jin L. Effect of Jiangtang Xiaozhi capsule on morphological changes of islet and liver in rat model [corrected] of type 2 diabetes [corrected] mellitus. Zhongguo Zhong Yao Za Zhi. 2008; 33:1067–1071. [PubMed: 18652360]

Highlights

- MALDI imaging mass spectrometry detected altered temporal lobe white matter lipid profiles in an intracerebral streptozotocin (i.c.-STZ) model of sporadic Alzheimer's disease.
- The main effects of i.c.-STZ were to increase temporal lobe white matter abundance of sulfatides and decrease phospholipids.
- The broad and striking abnormalities in lipid ion profiles could be used to assess Alzheimer-type white matter neurodegeneration.

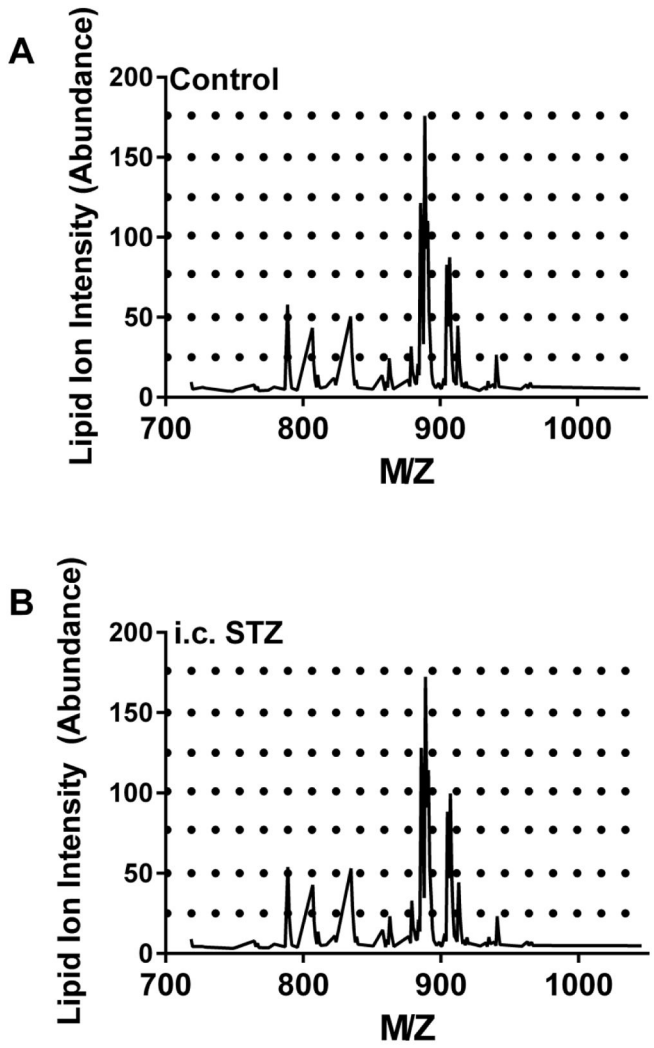

Figure 1.

Relative lipid ion intensity profiles in frontal WM. Lipid ion m/z and intensity were detected by MALDI-TOF. The spectra show relative intensities of lipid ions between m/z 600–1200 Da in controls compared with the i.c. STZ.

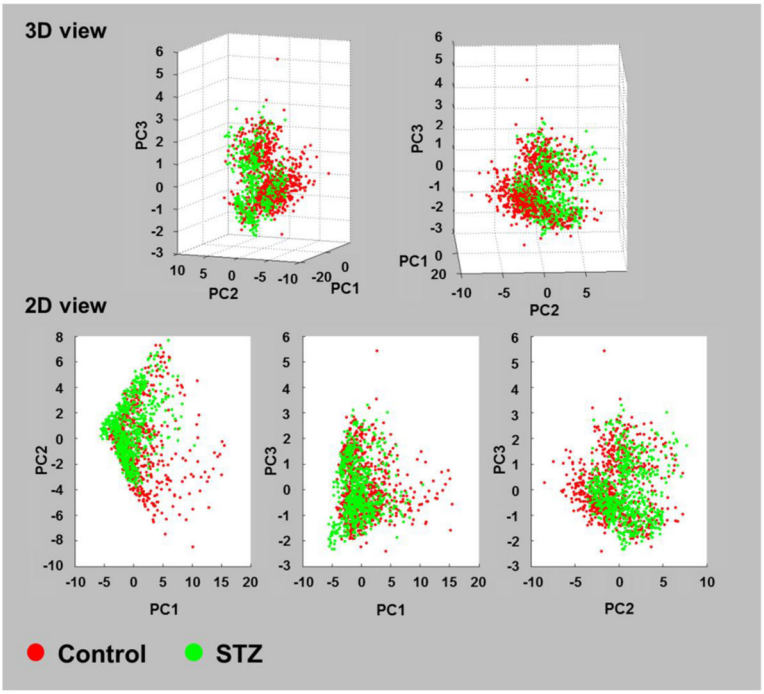

Figure 2.

Principal component analysis (PCA) of IMS data acquired in the negative-ionization mode. ClinProTools was used for PCA of the total MS spectra generated from temporal lobe WM ROIs in each group. Based on spectral similarities and WM lipid profiles, two distinct but overlapping clusters were identified corresponding to control (red) and i.c. STZ (green) samples. The incomplete overlap reflects the differential effects of i.c. STZ on temporal lobe lipid ion expression.

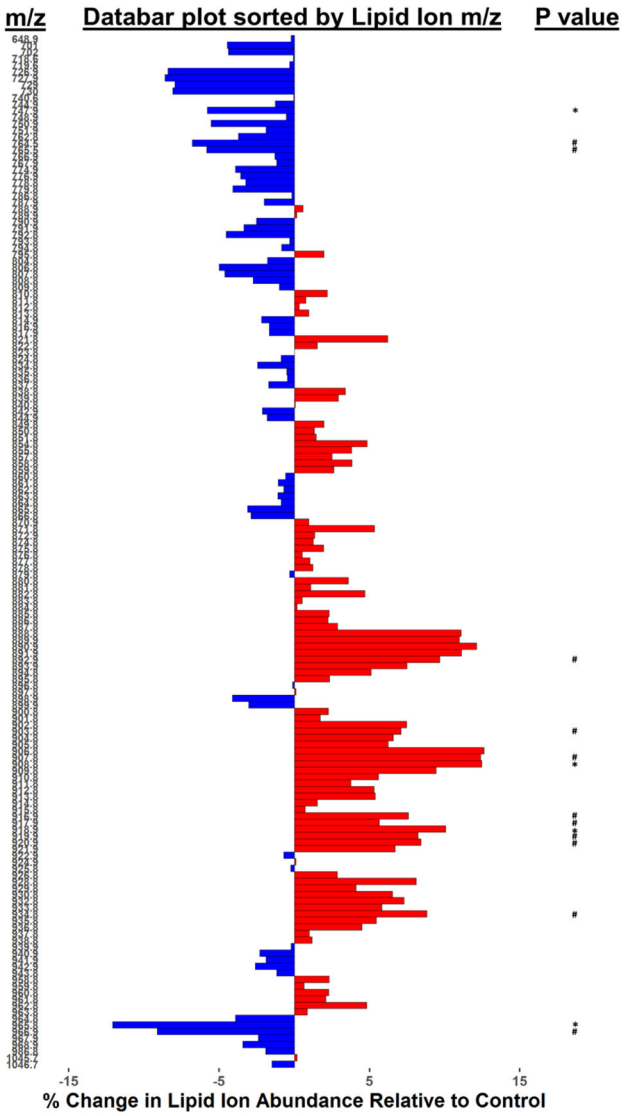

Fig. 3A

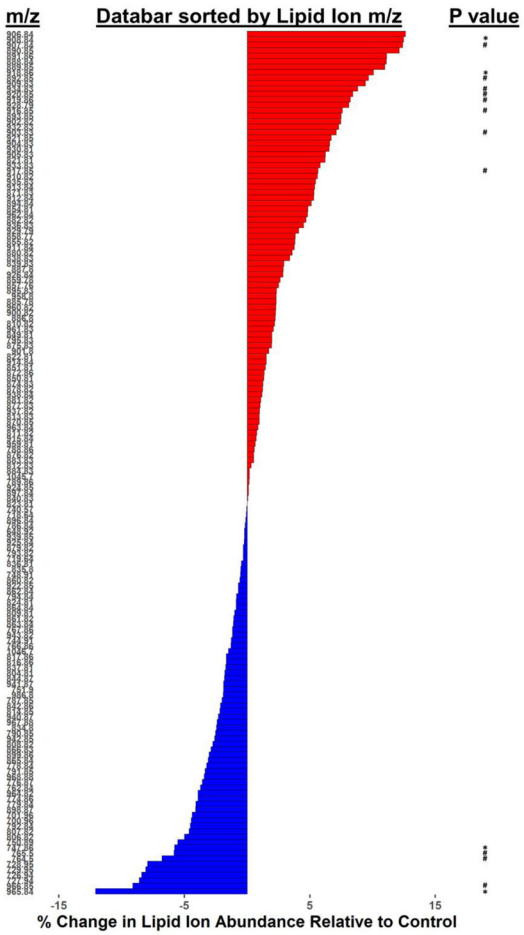

Fig. 3B

Figure 3.

Data bar plots illustrating effects of i.c. STZ on different lipid ion species. MALDI-IMS detected 158 distinct lipid ions in temporal lobe WM of both control and i.c. STZ treated rats. Calculated mean percentage changes in lipid ion levels measured in i.c. STZ relative to control are plotted. Bars to the left of the vertical axis reflect i.c. STZ-associated reductions in lipid ion expression, whereas bars to the right correspond to increased relative expression. The scale bar depicts the range of responses. (A) Data are sorted from lowest to highest m/z. (B) Data are sorted from the largest percentage increase to the largest percentage reduction in lipid ion expression in i.c. STZ relative to control white matter. Results of repeated measures T-test analysis (with 5% false discovery correction) are shown: # 0.10>P>0.05; *P<0.05. See Tables 3A and 3B for m/z values and lipid identifications.

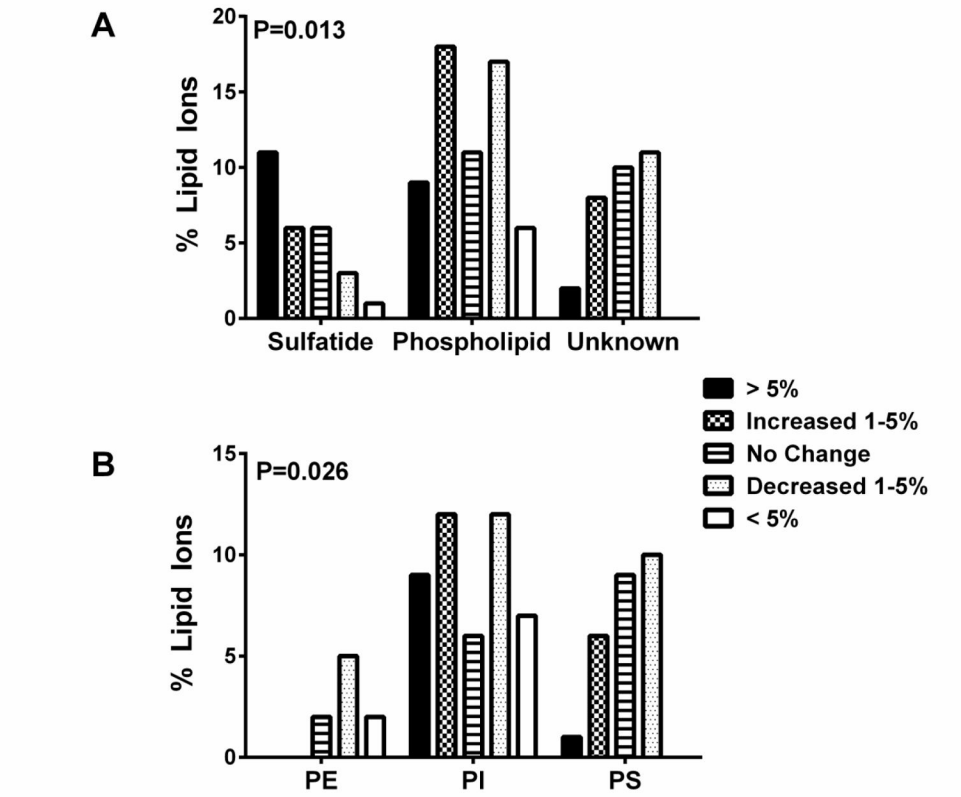

C

Comparisons	Inc >5%	Inc 1-5%	NC	Dec 1-5%	Dec >5%
ST Ph Ukn	P=0.048	P=0.027	N.S.	P=0.01	P=0.014
ST Ph	P=0.10	P<0.0001	P=0.10	P<0.0001	P=0.04
PE PI PS	P=0.0009	P=0.003	P=0.11	N.S.	P=0.015

Figure 4.

Summary effects of i.c. STZ on lipid ion expression. The aggregate effects i.c. STZ on the expression levels of different lipid sub-classes relative to control were evaluated. The percentages of lipid subtypes that were increased by >5%, between 1% and 5%, < 1%, or decreased between 1% and 5% or decreased > 5% are depicted graphically. Inter-group comparisons were made for (A) sulfatides (ST), all phospholipids (Ph), and unknown (unidentified; Ukn) lipids, and (B) the three main subtypes of phospholipids expressed, phosphatidylethanolamines (PE), phosphatidylinositols (PI), and phosphatidylserines (PS). Chi-square test results (P-values) are shown in the panels. (C) Fractional Chi-Square tests were used to determine which effects of i.c. STZ were significant or reached a statistical trend. The corresponding P-values are tabulated for comparisons among ST, Ph and Ukn, between ST and Ph, and among the 3 dominant Ph's: PE, PI and PS.

Table 1

Differential Expression of White Matter Lipids in Brains of i.c. STZ-treated Rats

m/z	Lipid Identification	Differential Expression
702.93	1) PS(30:2); 2) PS(P-31:1)	Control
766.46	PE(38:4)	i.c. STZ
768.48	PE(38:3)	i.c. STZ
796.77	ST(34:0)(OH) Carter	i.c. STZ
832.76	PS(40:7)	i.c. STZ
852.76	PS(42:11)	i.c. STZ
931.76	1) PI(41:2); 2) PI(42:9)	i.c. STZ
988.75	Not Identified (Unknown)	i.c. STZ

Lipids differentially expressed in only control or only i.c. STZ temporal lobe white matter. Lipid assignments were made using the LIPIDMAPS database or based on previously published MS/MS data.

Table 2

Temporal Lobe White Matter Lipid Composition

Lipids	Number (%) Identified
All Sulfatides	**39 (24.7%)**
Sulfatides	27 (69.2%)
C13-Sulfatides	12 (30.8%)
All Ceramides	**3 (2.0%)**
Ceramides	2 (67.0%)
C13-Ceramides	1 (33.0%)
All Phospholipids	**86 (54.4%)**
Phospholipids	61 (70.9%)
C13-Phospholipids	25 (29.1%)
Not Identified	**30 (19.0%)**

Temporal lobe WM lipids were evaluated by MALDI-IMS and lipid assignments were made using the LIPIDMAPS database or MS/MS results in previous publications.

Table 3A

STZ-Induced Changes in Lipid Ion Expression-Sorted by m/z

m/z	% Change	Lipid Identification	T-Test
648.92	−0.211	PS(26:1)	
700.96	−4.458	PE-p(34:1)	
701.96	−4.393	C13 isotope of PE-p(34:1)	
718.64	−0.080	PE(34:0)	
719.64	−0.314	PG(32:1)	
726.94	−8.396	PlsEtn(36:2)	
727.94	−8.607	C13 isotope of PlsEtn(36:2)	
728.95	−7.927	PlsEtn(36:1)	
729.95	−8.097	C13 isotope of PlsEtn(36:1)	
740.57	−0.052	PE(36:3)	
744.91	−1.275	PE(36:1)	
747.86	−5.786	PG(34:1)	*
748.91	−0.544	PlsEtn(38:5)	
750.89	−5.527	PlsEtn(38:4)	
751.9	−1.879	C13 isotope of PlsEtn(38:4)	
762.84	−3.727	Unknown	
764.5	−6.799	PE(38:5)	#
765.5	−5.842	C13 isotope of PE(38:5)	#
766.86	−1.305	PE(38:4)	
767.86	−1.182	C13 isotope of PE(38:4)	
774.86	−3.925	PlsEtn(40:7)	
776.87	−3.569	ST(34:2)	
778.84	−3.219	PlsEtn(40:5) or ST(34:1)	
779.84	−4.089	C13 isotope of PlsEtn(40:5) or ST(34:1)	
786.84	−0.168	PS(36:2)	
787.85	−2.016	C13 isotope of PS(36:2)	
788.86	0.565	PS(36:1)	
789.86	0.147	C13 isotope of PS(36:1)	
790.85	−2.513	PS(36:0)	
791.85	−3.358	C13 isotope of PS(36:0)	
792.84	−4.520	ST(34:2)(OH)	
793.82	−0.311	Unknown	
794.84	−0.850	ST(34:1)(OH)	
795.83	1.955	PI(O-32:0)	
804.81	−1.796	ST(36:2)	
806.82	−4.998	ST(36:1)	
807.82	−4.640	PI(32:1)	
808.82	−2.749	PS(38:5)	
809.81	−0.993	C13 isotope of PS(38:5)	

m/z	% Change	Lipid Identification	T-Test
810.82	2.192	PS(38:4)	
811.82	0.755	C13 isotope of PS(38:4)	
812.83	0.314	PS(38:3)	
813.83	0.974	C13 isotope of PS(38:3)	
814.85	−2.168	PS(38:2)	
816.86	−1.663	PS(38:1)	
817.86	−1.650	C13 isotope of PS(38:1)	
821.81	6.198	PG(40:6)	
822.81	1.538	ST(36:1)(OH)	
823.81	0.000	ST(36:1)(2OH)	
824.81	−0.865	C13 isotope of ST(36:1)(2OH)	
834.8	−2.450	PS(40:6)	
835.8	−0.505	PI(34:1)	
836.81	−0.458	C13 isotope of PI(34:1)	
837.81	−1.710	PI(34:0)	
838.83	3.385	PS(40:4)	
839.83	2.921	C13 isotope of PS(40:4)	
840.83	0.045	isotope of PS(40:4)	
842.86	−2.119	Unknown	
844.87	−1.797	PS(40:1)	
849.81	1.956	PI(O-36:1) or PI(P-36:0)	
850.81	1.335	ST(20:0)(OH)	
851.81	1.464	C13 isotope of ST(20:0)(OH)	
854.81	4.841	Unknown	
855.82	3.806	PI(36:5)	
857.76	2.509	PI(36:4)	
858.77	3.839	C13 isotope of PI(36:4)	
859.78	2.639	PI(36:3)	
860.82	−0.575	ST(40:2)	
861.82	−1.068	PI(36:2)	
862.84	−0.701	ST(40:1)	
863.84	−1.099	PI(36:1)	
864.84	−0.878	ST(40:0)	
865.84	−3.110	PI(36:0)	
866.83	−2.884	C13 isotope of PI(36:0)	
870.85	0.967	Unknown	
871.83	5.318	PI(O-38:4) or PI(P-38:3)	
872.86	1.359	Unknown	
874.83	1.260	ST(40:3)(OH)	
875.83	1.954	C13 isotope of ST(40:3)(OH)	
876.82	0.523	ST(40:2)(OH)	
877.83	1.041	C13 isotope of ST(40:2)(OH)	

m/z	% Change	Lipid Identification	T-Test
878.82	1.220	ST(40:1)(OH)	
879.82	−0.302	C13 isotope of ST(40:1)(OH)	
880.82	3.595	ST(40:0)(OH)	
881.82	1.095	PI(38:6)	
882.82	4.682	Unknown	
883.83	0.521	PI(38:5)	
884.83	0.181	C13 isotope of PI(38:5)	
885.78	2.301	PI(38:4)	
886.8	2.233	ST(42:3)	
887.8	2.883	PI(38:3)	
888.84	11.081	ST(42:2)	
889.85	10.969	PI(38:2)	
890.85	12.117	ST(42:1)	
891.86	11.120	PI(38:1)	
892.85	9.678	C13 isotope of PI(38:1)	#
893.85	7.478	PI(38:0)	
894.84	5.099	C13 isotope of PI(38:0)	
895.83	2.331	isotope of PI(38:0)	
896.84	−0.114	Unknown	
897.84	0.111	Unknown	
898.87	−4.116	Unknown	
899.86	−3.044	Unknown	
900.82	2.271	PS(44:1)	
901.8	1.730	Unknown	
902.82	7.462	ST(42:3)(OH)	
903.83	7.089	C13 isotope of ST(42:3)(OH)	#
904.83	6.585	ST(42:2)(OH)	
905.83	6.238	C13 isotope of ST(42:2)(OH)	
906.84	12.618	ST(42:1)(OH)	
907.84	12.381	C13 isotope of ST(42:1)(OH)	#
908.84	12.468	ST(42:0)(OH)	*
909.83	9.425	PI(40:6)	
910.82	5.594	PS(46:11)	
911.84	3.761	PI(40:5)	
912.84	5.290	LacCer(d38:3)	
913.84	5.383	PI(40:4)	
914.84	1.535	LacCer(d38:2)	
915.84	0.723	C13 isotope of LacCer(d38:2)	
916.85	7.578	ST(44:2)	#
917.85	5.649	C13 isotope of ST(44:2)	#
918.86	10.051	ST(44:1)	*
919.86	8.219	C13 isotope of ST(44:1)	#

m/z	% Change	Lipid Identification	T-Test
920.85	8.404	ST(44:0)	#
921.85	6.712	C13 isotope of ST(44:0)	
922.85	−0.694	Unknown	
924.85	0.115	Unknown	
925.84	−0.239	Unknown	
926.84	2.841	Unknown	
928.79	8.098	Unknown	
929.79	4.102	PI(42:10)	
930.81	6.528	Unknown	
932.83	7.300	ST(44:1)(OH)	
933.83	5.819	C13 isotope of ST(44:1)(OH)	
934.83	8.812	ST(44:0)(OH)	#
935.83	5.451	PIP(36:5)	
936.83	4.490	PS(48:12)	
937.82	0.994	Unknown	
938.84	1.186	PS(48:11)	
939.85	−0.225	C13 isotope of PS(48:11)	
940.87	−2.290	Unknown	
941.87	−1.873	Unknown	
942.85	−2.586	Unknown	
943.82	−1.182	Unknown	
958.8	2.301	Phospholipid	
959.81	0.635	Unknown	
960.82	2.280	Unknown	
961.83	2.091	Unknown	
962.84	4.804	Phospholipid	
963.84	0.866	Unknown	
964.82	−3.908	Unknown	
965.84	−12.094	PIP(38:4)	*
966.85	−9.122	C13 isotope of PIP(38:4)	#
967.88	−2.403	PIP(38:3)	
968.88	−3.436	Unknown	
986.8	−1.917	Unknown	
1045.7	0.178	PIP2(38:4)	
1046.7	−1.485	C13 Isotope of PIP2(38:4)	

The table lists the m/z's of all lipid ions identified in both control and i.c. STZ white matter samples, the calculated mean percentage differences in lipid ion abundance between i.c. STZ and control, the assignment of each lipid, and results of repeated measures T-test analysis (with 5% false discovery correction). The data are sorted from lowest to highest m/z.

0.10>P>0.05;

* P<0.05.

These results are graphically depicted in Figure 3A.

Table 3B

STZ-Induced Changes in Lipid Ion Expression-Sorted by Percent Difference from Control

m/z	% Change	Lipid Identification	T-Test
906.84	12.618	PIP(38:4)	
908.84	12.468	C13 isotope of PIP(38:4)	*
907.84	12.381	C13 isotope of PlsEtn(36:2)	#
890.85	12.117	PlsEtn(36:2)	
891.86	11.120	C13 isotope of PlsEtn(36:1)	
888.84	11.081	PlsEtn(36:1)	
889.85	10.969	PE(38:5)	
918.86	10.051	C13 isotope of PE(38:5)	*
892.85	9.678	PG(34:1)	#
909.83	9.425	PlsEtn(38:4)	
934.83	8.812	ST(36:1)	#
920.85	8.404	PI(32:1)	#
919.86	8.219	ST(34:2)(OH)	#
928.79	8.098	PE-p(34:1)	
916.85	7.578	C13 isotope of PE-p(34:1)	#
893.85	7.478	Unknown	
902.82	7.462	C13 isotope of PlsEtn(40:5) or ST(34:1)	
932.83	7.300	PlsEtn(40:7)	
903.83	7.089	Unknown	#
921.85	6.712	Unknown	
904.83	6.585	ST(34:2)	
930.81	6.528	Unknown	
905.83	6.238	C13 isotope of PS(36:0)	
821.81	6.198	PlsEtn(40:5) or ST(34:1)	
933.83	5.819	PI(36:0)	
917.85	5.649	Unknown	#
910.82	5.594	C13 isotope of PI(36:0)	
935.83	5.451	PS(38:5)	
913.84	5.383	Unknown	
871.83	5.318	PS(36:0)	
912.84	5.290	PS(40:6)	
894.84	5.099	PIP(38:3)	
854.81	4.841	Unknown	
962.84	4.804	PS(38:2)	
882.82	4.682	Unknown	
936.83	4.490	C13 isotope of PS(36:2)	
929.79	4.102	Unknown	
858.77	3.839	C13 isotope of PlsEtn(38:4)	
855.82	3.806	Unknown	

m/z	% Change	Lipid Identification	T-Test
911.84	3.761	PS(40:1)	
880.82	3.595	ST(36:2)	
838.83	3.385	PI(34:0)	
839.83	2.921	PS(38:1)	
887.8	2.883	C13 isotope of PS(38:1)	
926.84	2.841	C13 Isotope of PIP2(38:4)	
859.78	2.639	PE(38:4)	
857.76	2.509	PE(36:1)	
895.83	2.331	Unknown	
958.8	2.301	C13 isotope of PE(38:4)	
885.78	2.301	PI(36:1)	
960.82	2.280	PI(36:2)	
900.82	2.271	C13 isotope of PS(38:5)	
886.8	2.233	ST(40:0)	
810.82	2.192	C13 isotope of ST(36:1)(2OH)	
961.83	2.091	ST(34:1)(OH)	
849.81	1.956	ST(40:1)	
795.83	1.955	Unknown	
875.83	1.954	ST(40:2)	
901.8	1.730	PlsEtn(38:5)	
822.81	1.538	PI(34:1)	
914.84	1.535	C13 isotope of PI(34:1)	
851.81	1.464	PG(32:1)	
872.86	1.359	Unknown	
850.81	1.335	C13 isotope of ST(40:1)(OH)	
874.83	1.260	Unknown	
878.82	1.220	C13 isotope of PS(48:11)	
938.84	1.186	PS(26:1)	
881.82	1.095	PS(36:2)	
877.83	1.041	Unknown	
937.82	0.994	PE(34:0)	
813.83	0.974	PE(36:3)	
870.85	0.967	ST(36:1)(2OH)	
963.84	0.866	isotope of PS(40:4)	
811.82	0.755	Unknown	
915.84	0.723	Unknown	
959.81	0.635	C13 isotope of PS(36:1)	
788.86	0.565	PIP2(38:4)	
876.82	0.523	C13 isotope of PI(38:5)	
883.83	0.521	PS(38:3)	
812.83	0.314	PI(38:5)	
884.83	0.181	ST(40:2)(OH)	

m/z	% Change	Lipid Identification	T-Test
1045.7	0.178	PS(36:1)	
789.86	0.147	Unknown	
924.85	0.115	C13 isotope of LacCer(d38:2)	
897.84	0.111	C13 isotope of PS(38:4)	
840.83	0.045	Unknown	
823.81	0.000	Unknown	
740.57	−0.052	C13 isotope of PS(38:3)	
718.64	−0.080	Unknown	
896.84	−0.114	C13 isotope of ST(40:2)(OH)	
786.84	−0.168	PI(38:6)	
648.92	−0.211	PS(48:11)	
939.85	−0.225	ST(40:1)(OH)	
925.84	−0.239	ST(40:3)(OH)	
879.82	−0.302	ST(20:0)(OH)	
793.82	−0.311	Unknown	
719.64	−0.314	C13 isotope of ST(20:0)(OH)	
836.81	−0.458	LacCer(d38:2)	
835.8	−0.505	ST(36:1)(OH)	
748.91	−0.544	Unknown	
860.82	−0.575	C13 isotope of ST(40:3)(OH)	
922.85	−0.694	PI(O-32:0)	
862.84	−0.701	PI(O-36:1) or PI(P-36:0)	
794.84	−0.850	Unknown	
824.81	−0.865	PS(38:4)	
864.84	−0.878	ST(42:3)	
809.81	−0.993	PS(44:1)	
861.82	−1.068	Unknown	
863.84	−1.099	PI(38:4)	
767.86	−1.182	Phospholipid	
943.82	−1.182	isotope of PI(38:0)	
744.91	−1.275	PI(36:4)	
766.86	−1.305	PI(36:3)	
1046.7	−1.485	Unknown	
817.86	−1.650	PI(38:3)	
816.86	−1.663	C13 isotope of PS(40:4)	
837.81	−1.710	PS(40:4)	
804.81	−1.796	ST(40:0)(OH)	
844.87	−1.797	PI(40:5)	
941.87	−1.873	PI(36:5)	
751.9	−1.879	C13 isotope of PI(36:4)	
986.8	−1.917	PI(42:10)	
787.85	−2.016	PS(48:12)	

m/z	% Change	Lipid Identification	T-Test
842.86	−2.119	Unknown	
814.85	−2.168	Phospholipid	
940.87	−2.290	Unknown	
967.88	−2.403	C13 isotope of PI(38:0)	
834.8	−2.450	LacCer(d38:3)	
790.85	−2.513	PI(O-38:4) or PI(P-38:3)	
942.85	−2.586	PI(40:4)	
808.82	−2.749	PIP(36:5)	
866.83	−2.884	PS(46:11)	
899.86	−3.044	C13 isotope of ST(44:2)	
865.84	−3.110	C13 isotope of ST(44:1)(OH)	
778.84	−3.219	PG(40:6)	
791.85	−3.358	C13 isotope of ST(42:2)(OH)	
968.88	−3.436	Unknown	
776.87	−3.569	ST(42:2)(OH)	
762.84	−3.727	C13 isotope of ST(44:0)	
964.82	−3.908	C13 isotope of ST(42:3)(OH)	
774.86	−3.925	ST(44:1)(OH)	
779.84	−4.089	ST(42:3)(OH)	
898.87	−4.116	PI(38:0)	
701.96	−4.393	ST(44:2)	
700.96	−4.458	Unknown	
792.84	−4.520	C13 isotope of ST(44:1)	
807.82	−4.640	ST(44:0)	
806.82	−4.998	ST(44:0)(OH)	
750.89	−5.527	PI(40:6)	
747.86	−5.786	C13 isotope of PI(38:1)	*
765.5	−5.842	ST(44:1)	#
764.5	−6.799	PI(38:2)	#
728.95	−7.927	ST(42:2)	
729.95	−8.097	PI(38:1)	
726.94	−8.396	ST(42:1)	
727.94	−8.607	C13 isotope of ST(42:1)(OH)	
966.85	−9.122	ST(42:0)(OH)	#
965.84	−12.094	ST(42:1)(OH)	*

The table lists the m/z's of all lipid ions identified in both control and i.c. STZ white matter samples, the calculated mean percentage differences in lipid ion abundance between i.c. STZ and control, the assignment of each lipid, and results of repeated measures T-test analysis (with 5% false discovery correction). The data are sorted from the largest percentage increase to the largest percentage reduction in lipid expression observed in the i.c. STZ relative to control white matter.

0.10>P>0.05;

* P<0.05.

These results are graphically depicted in Figure 3B.

Table 4

Effects of i.c. STZ on Lipid Ion Characteristics in Temporal Lobe White Matter

	i.c. STZ Effects Relative to Control				
Lipid	**Increased >5%**	**Increased 1–5%**	**No Change (< 1%)**	**Decreased 1–5%**	**Decreased >5%**
All Sulfatides	**18 (46.2%)**	**9 (23.1%)**	**8 (20.5%)**	**3 (7.7%)**	**1 (2.6%)**
Sulfatide	11 (40.7%)	6 (22.2%)	6 (22.2%)	3 (11.1%)	1 (3.7%)
C13-Sulfatide	7 (58.3%)	3 (27.3%)	2 (7.4%)	0	0
All Ceramides	**1 (33.3%)**	**1 (33.3%)**	**1 (33.3%)**	**0**	**0**
Ceramide	1 (50.0%)	1 (50.0%)	0	0	0
C13-Ceramide	0	0	1 (100%)	0	0
All Phospholipids	**11 (12.8%)**	**20 (23.3%)**	**18 (20.9%)**	**27 (31.4%)**	**10 (11.6%)**
Phospholipid	9 (14.8%)	18 (29.5%)	11 (18.0%)	17 (27.9%)	6 (9.8%)
C13-Phospholipid	2 (8.0%)	2 (8.0%)	7 (28.0%)	10 (40.0%)	4 (16.0%)
Unidentified	**2 (6.7%)**	**8 (26.7%)**	**9 (30.0%)**	**11 (36.7%)**	**0 (0.00)**
Total (158)	**32 (20.3%)**	**38 (23.4%)**	**36 (24.1%)**	**41 (25.9%)**	**11 (7.0%)**

The i.c. STZ-mediated mean percentage change in temporal lobe white matter lipid ion expression was calculated for each lipid (n=8 samples/group). The effect sizes were binned with respect to the magnitude (greater than 5%, 1–5%, less than 1%) and direction (stimulatory versus inhibitory) of change relative to control. The table shows the number (frequency) of distinct lipid ions within each subtype exhibiting different response levels. Chi-square analysis of the proportions of sulfatides and phospholipids (including C13 isotopes and excluding ceramides and unidentified lipids) demonstrated that i.c. STZ treatments caused disproportional increases in sulfatides and reductions in phospholipids relative to control (Pearson's Chi-Square=24.72; P=0.00006).